Progress In Electromagnetics Research B, Vol. 58, 181–191, 2014

Design of a Compact Ultra-Wide Band Bow-Tie Slot Antenna System for the Evaluation of Structural Changes in Civil Engineering Works

Florence Sagnard*

Abstract—A compact UWB bowtie-slot antenna ($36 \times 23\,\mathrm{cm}^2$) fed by a CPW transition is proposed for an improved ground-coupling radar. The antenna has an operating frequency band in the range $[0.46; 4]\,\mathrm{GHz}$. Full-wave modeling using the FDTD approach has allowed to study in details the antenna radiation characteristics in air and in the presence of a soil. Afterwards, a radar system made of a pair of independent shielded bowtie antennas has been considered to probe the sub-surface very close to the air-soil interface. The polarization diversity in the E and H-planes is an important aspect which has been studied in order to further detect the orientation of damages (cracks, delaminations ...) in civil engineering structures. Measurements in a dry and wet sand in different system configurations have allowed to first characterize the GPR system and to draw comparisons with numerical results. The ability of the radar to detect small buried objects has been investigated.

1. INTRODUCTION

In the last decade, the recent development of an Ultra-Wide Band (UWB) Ground Penetrating Radar (GPR) as a non-invasive sensing tool for soils or man-made structures has opened opportunities to provide more structural information and quantitative dielectric characteristics [1–3]. As our applications are mainly concerned with civil engineering to perform supervision, inventory, and soil characterization, improvements are needed in resolution and depth penetration. In general, a GPR system is composed of a pair of antennas (bistatic system), one for transmission and the other one for reception, that are moved linearly above the soil surface to scan non-destructively the sub-surface. In this study, a stepped-frequency continuous wave (SFCW) radar, working from 460 MHz to beyond 4 GHz in air and operating very close (a few cm) to the ground surface has been designed. As compared to air-coupled radar that suffers from a significant reflection at the ground interface, ground-coupled radar increases energy transfer of electromagnetic radiation in the sub-surface and penetration depth. On a common soil ($\varepsilon'_s = 5.5$; $\sigma_s = 0.01\,\mathrm{S \cdot m^{-1}}$), we hope that the lower frequency is close to 250 MHz. The major key component in the present GPR system is the antenna geometry and its radiation characteristics; it has to operate in an UWB, show a compact size to be used easily on sites, and shall not have a late-time ringing phenomenon in its time response that will cause the deterioration in the down range resolution of the system.

Since the burst in 2002 of the UWB technology for communication systems in the $[3.1; 10.6]\,\mathrm{GHz}$ frequency range, microstrip patch antennas (MPAs) have reached a sufficient maturity which has allowed to design many types of planar antennas that offer several advantages such as compact size, low-cost, ease of fabrication, lightweight, and various shapes. Thus, we have adapted this planar technology to design an original triangle bowtie slot antenna on a FR4 substrate ($h = 1.5\,\mathrm{mm}$, $\varepsilon'_r = 4.4$; $\tan\delta = 0.01$)

Received 30 January 2014, Accepted 18 February 2014, Scheduled 24 February 2014

* Corresponding author: Florence Sagnard (florence.sagnard@ifsttar.fr).
The author is with the Department COSYS, University Paris-Est, IFSTTAR, 14-20, Bd Newton, Champs-sur-Marne 77420, France.

at lower frequencies with reduced dimensions close to the A4 sheet size [4–9]. A tapered coplanar waveguide (CPW) transmission line with a 50 Ω impedance at the antenna frontier has been defined. To eliminate undesirable reflections from the upper environment particularly at low frequencies, and reduce the coupling between the transmitting and the receiving units, a partial conductive shield only opened towards the ground and coated with an inner layered absorbing material has been added [9]. The aim of this study is to assess the acquisition configuration, and characterize the polarization of the antennas for the detection and discrimination of discontinuities with small lateral dimensions (less than 25 mm) in civil engineering works to further consider structural features such as cracks, repair patches, buried utility cuts [1, 3]. The development of direct full-wave modeling based on the finite difference time domain (FDTD) technique has allowed to study in details the UWB radiation properties of one antenna in the E and H-planes in air and in a common soil ($\varepsilon'_s = 5.5$; $\sigma_s = 0.01\ \mathrm{S{\cdot}m^{-1}}$). Afterwards, a parameter study associated with the geometrical configuration of the bistatic radar link in both polarizations and on a common soil has allowed to characterize the transmission link. Measurements have been made in the frequency domain, using a vector network analyzer (VNA) in the range [0.05; 4] GHz on a dry and wet sand and they have been compared to numerical results. The radar system has also been preliminary evaluated in the detection of canonical objects in a wet sand.

2. TRIANGLE BOWTIE SLOT ANTENNA DESIGN

2.1. Antenna Geometry

As the triangle bow-tie slot antenna visualized in Figure 1 is intended to be positioned close to the soil surface, we have defined its overall dimensions to operate at low frequencies close to 250 MHz (return loss $S_{11\,\mathrm{dB}}(f) \leq -10\,\mathrm{dB}$) in the presence of a common dry soil with dielectric characteristics

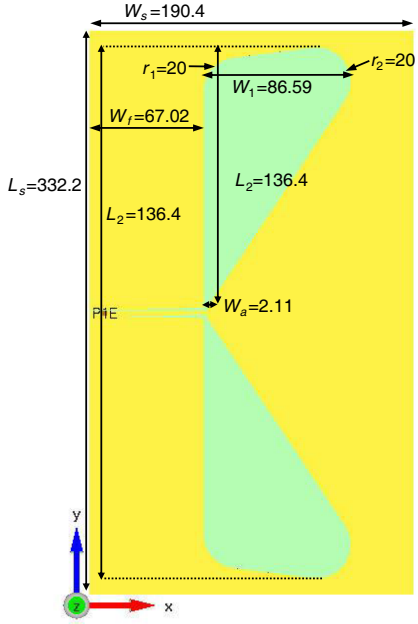

(a) CPW-fed triangle bow-tie slot antenna

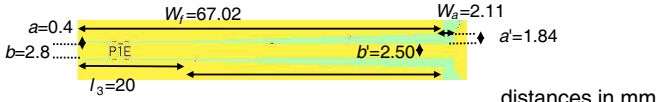

(b) tapered feed line

Figure 1. (a) Geometry of the triangle bowtie slot antenna modeled using FDTD simulations; (b) Top view of the tapered feed line (distances in mm).

$\varepsilon'_s = 5.5$; $\sigma_s = 0.01\,\mathrm{S \cdot m^{-1}}$. The radiation characteristics have been studied using numerical FDTD simulations (EMPIRE software). The antenna has been designed on a single-sided FR4 substrate ($h = 1.5\,\mathrm{mm}$ $\varepsilon'_r = 4.4$; $\tan\delta = 0.01$, $35\,\mu\mathrm{m}$ copper-clad). The overall dimensions of the antenna are $W_s = 190.4\,\mathrm{mm}$ and $L_s = 332.2\,\mathrm{mm}$. The antenna is made of two rounded slot triangles ($W_1 = 86.59\,\mathrm{mm}$ and $L_1 = 276.47\,\mathrm{mm}$, radii r_1 and $r_2 = 20\,\mathrm{mm}$) fed by a tapered CPW line with length $W_f = 67.02\,\mathrm{mm}$ [8]. It is fed in port 1 from a SMA (subminiature version A) connector connected to a $50\,\Omega$ CPW line with $a = 0.4\,\mathrm{mm}$ and $b = 2.8\,\mathrm{mm}$. The antenna feed line is tapered for impedance matching with dimensions at the feed-point $a' = 1.84\,\mathrm{mm}$ and $b' = 2.50\,\mathrm{mm}$ [7].

The surface current distribution j_{xy} on the antenna at the frequency 450 MHz and visualized in Figure 2 highlights that the slot antenna has a principal radiation along axis Ox. A null is observed at the front end in the middle of the antenna along axis Oy. Thus, the directional radiation characteristic will be suitable for dual polarizations studies. To eliminate backward radiations in air induced by the close environment, and to reduce the direct coupling between the transmitting and receiving antennas in the GPR system, each antenna has been enclosed in a perfectly conductive box opened towards the ground surface as shown in Figure 3; the conductive box (height $h_c = 67.5\,\mathrm{mm}$, width $W_c = 231\,\mathrm{mm}$, and length $L_c = 362\,\mathrm{mm}$) has been filled in the simulations with a three layered absorbing material which is supposed to progressively absorb the electromagnetic waves and to reduce multiple reflections inside the cavity; consequently, the return loss in all the operating frequency band is slightly modified The planar absorbing material has been modeled according to Atteia's work that has considered a conductivity profile following the law $\sigma = 10^{n-3}\,\mathrm{S \cdot m^{-1}}$, where n is the layer number, and $n = 1$ is the layer just in contact with the antenna [9]. Thus, according to a parametric study not presented here, the characteristics of the absorbing layers are finally: $\varepsilon_{1,2,3} = 1.5$, $\sigma_1 = 0.01\,\mathrm{S \cdot m^{-1}}$; $e_1 = 24.2\,\mathrm{mm}$; $\sigma_2 = 0.1\,\mathrm{S \cdot m^{-1}}$; $e_2 = 29.3\,\mathrm{mm}$ and $\sigma_3 = 1\,\mathrm{S \cdot m^{-1}}$; $e_3 = 14\,\mathrm{mm}$. As shown in Figure 3, the front and also the printed face of the antenna is supposed to be positioned towards the soil surface at an elevation h close to 10 mm to better match the soil impedance and to consider potential irregularities on the soil surface.

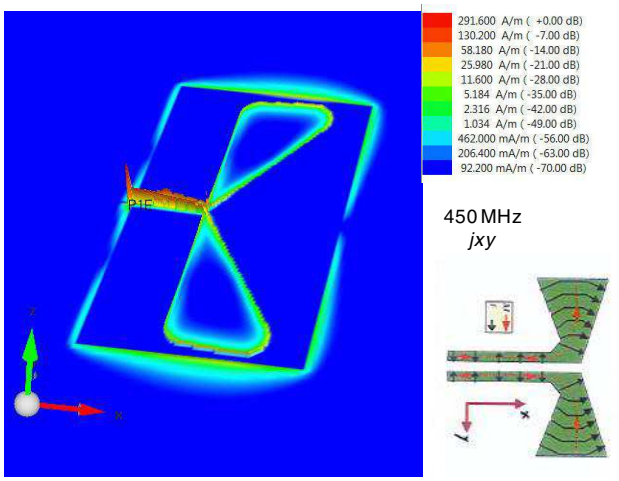

Figure 2. Surface current distribution j_{xy} on the antenna at the frequency 450 MHz.

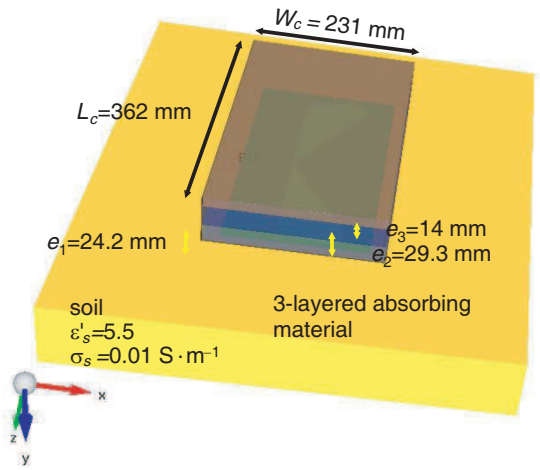

Figure 3. Geometry of the shielded slot bowtie modeled using FDTD simulations.

2.2. Theoretical Parameter Study

Main parameters which influence significantly the reflection coefficient $S_{11\,\mathrm{dB}}(f)$ such as a' and l_3 (feed-line), W_1 (triangle width), L_s, and W_s (substrate dimensions) have been studied to define the final antenna geometry as compact as possible. The operating frequency band extends beyond 4 GHz, but the higher frequencies will not penetrate sufficiently into the soil to extract reflection signals from buried discontinuities.

Firstly, the antenna has been studied alone in air. As shown in Figure 4(a), the increase of the arm length L_1 from 136.4 (original) to 148.1 mm does not significantly modify the lower operating frequency (S_{11} (dB) < -10 dB) but increases the S_{11} (dB) amplitude between 0.870 and 3.5 GHz. A compromise between the total arms length L_1 and width W_1 has to be found to extend the bandwidth towards lower frequencies while keeping a compact geometry. A width variation of around 8 mm as compared to the original one shows that a higher value ($W_1 = 94.84$ mm) is responsible for a decrease of S_{11} (dB) until 2.4 GHz, but an increase is observed afterwards. A width decrease ($W_1 = 78.66$ mm) increases S_{11} (dB) until 2.5 GHz, and between 2.8 and 3.7 GHz. These observations justify the choice for $W_1 = 86.9$ mm. Then, the main influential feed-line parameters l_3 and a' on S_{11} (dB) whose values have been changed from 20 to 27 mm and from 2.5 to 2.7 mm respectively such as visualized in Figure 4(b) show both an increase in amplitude from 2.2 to 3.3 GHz. Few changes are observed below 1 GHz. Parameter a' seems to induce significant change in the antenna impedance matching to the connector 50 Ω. Moreover, the influence of substrate length L_s and width W_s has been studied to reduce significantly the dimensions of the antenna. The results visualized in Figure 5(a) show that if W_s is changed from 190.4 to 185 mm, the return loss increases at the frequency 0.722 GHz, that corresponds to the higher amplitude inside the bandwidth and close to -10 dB; thus $W_s = 190.4$ mm has been defined. Concerning the substrate length L_s, we have remarked that the value 332.2 mm gives a slightly lower return loss amplitude between 0.863 and 1.6 GHz than the value 342 mm that explains the choice made for the lower value.

Afterwards, the structure of a partial shied has been studied in order to modify slightly the S_{11} (dB) amplitude in the overall bandwidth. Using a three layered absorbing material, FDTD simulations based

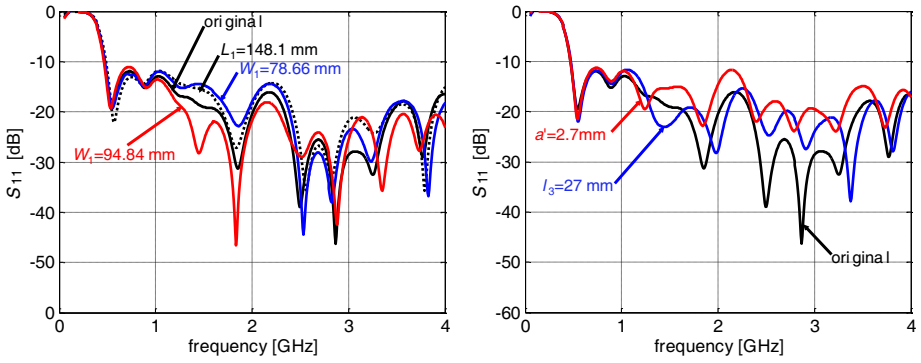

(a) parameters arm length and width (b) feed-line parameters

Figure 4. Influence of antenna geometrical parameters on the return loss $S_{11\,\mathrm{dB}}(f)$; (a) Arm length and width; (b) Feed-line.

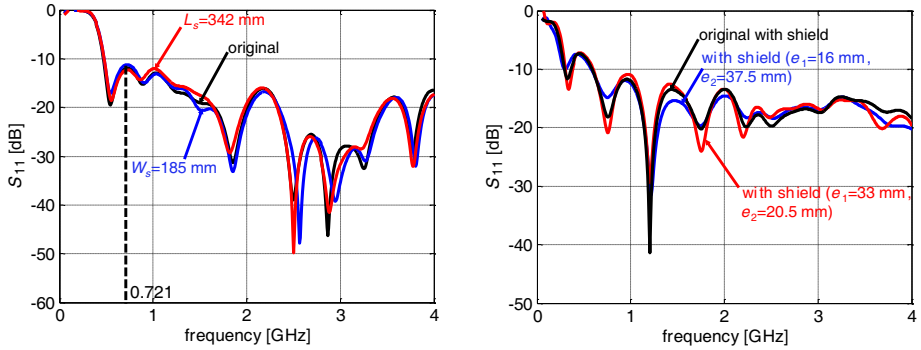

(a) parameters substrate length and width (b) parameters of the three-layered absorbing material

Figure 5. Influence of antenna geometrical parameters on the return loss $S_{11\,\mathrm{dB}}(f)$; (a) Substrate length and width; (b) The three-layered absorbing material.

on sensitivity analysis have helped us to design a compact conductive box with length $L_s = 432\,\text{mm}$, width $W_c = 356.5\,\text{mm}$ and height $h_s = 82.5\,\text{mm}$. Supposing that the overall height remains constant, the influence of the thicknesses associated with layers 1 and 2 (see Figure 3) has been studied; the results presented in Figure 5(b) show that a decrease of e_1 from the initial value 24.2 mm to 16 mm gives a S_{11} (dB) amplitude greater and lower as compared to the nominal value along all the bandwidth. When increasing e_1 to 33 mm, the S_{11} (dB) amplitude remains generally slightly higher as compared to the nominal case except for frequencies higher than 3.1 GHz that are quite high for GPR applications.

The comparison of antenna responses in terms of S_{11} (dB) amplitude, without and with a shield and collected in Figure 6, shows that the shield produces a shift towards the lower frequencies of the first frequency corresponding to S_{11} (dB) $= -10\,\text{dB}$ from 0.469 to 0.287 GHz. In general, we observe that the shield smoothes the S_{11} amplitude. Moreover, the higher amplitude situated in the operating bandwidth at 0.730 GHz reaches the amplitude $-7.36\,\text{dB}$, thus slightly higher than $-10\,\text{dB}$. In the presence of a common soil at an elevation $h = 1\,\text{cm}$ above the soil surface, we observe that the S_{11} (dB) amplitude associated with the shielded antenna decreases significantly as compared to the case in air at frequencies higher than 0.840 GHz. Moreover, we remark a slight shift on the left of the lower frequency corresponding to S_{11} (dB) $= -10$ from 0.287 to 0.250 GHz that is induced by the presence of the dielectric soil; the first resonant peak remains almost at the same position. Thus, a satisfactory antenna matching with the soil is obtained.

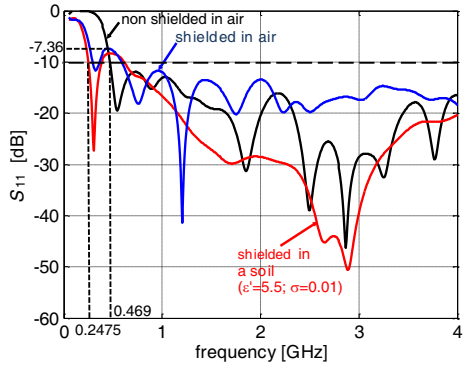

Figure 6. Theoretical return loss $S_{11\,\text{dB}}(f)$ without and with a shield, in air and in the presence of a common soil ($\varepsilon'_s = 5.5$; $\sigma_s = 0.01\,\text{S}\cdot\text{m}^{-1}$).

The radiation patterns of the shielded triangle bow-tie slot antenna in air at four frequencies 0.450, 0.800, 1, and 2 GHz are plotted in Figures 7(a), 7(b), 7(c), and 7(d) respectively in both planes E (xOz or $\phi = 0°$) and H (yOz or $\phi = 90°$). The backward radiation corresponds to the bottom half plane situated in the range $[-90°; 90°]$. In the E-plane, we remark that the component E_θ is dominant

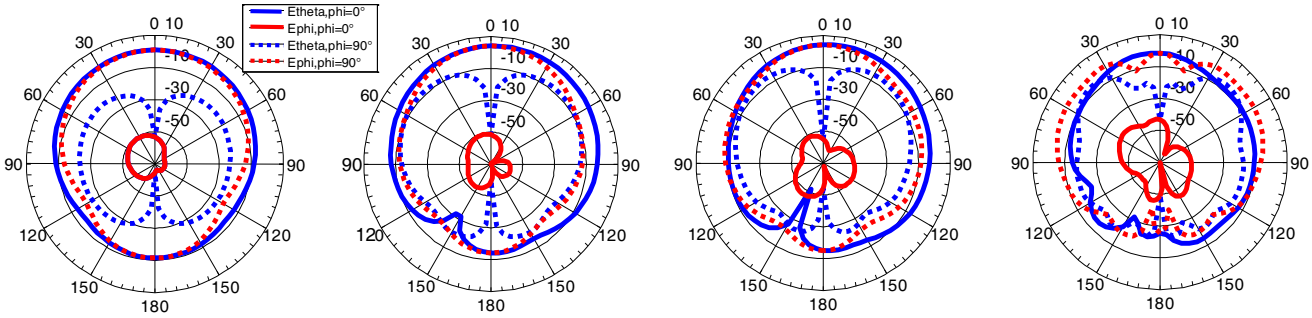

(a) 450 MHz (b) 800 MHz (c) 1 GHz (d) 2 GHz

Figure 7. Theoretical radiation patterns in both E and H-planes associated with the shielded slot bowtie antenna in air at frequencies 450 MHz, 800 MHz, 1 GHz, and 2 GHz.

and consequently the component E_ϕ can be assumed negligible; in air, without shield, the maximum gain is 5.4 dB at 0.800 GHz. In the the H-plane, we observe in Figures 7(a), 7(b), 7(c), and 7(d) a lower amplitude difference between both E-components in the angle range $[30°; 70°]$ and $[110°; 150°]$ at frequencies 0.8 and 1 GHz. In both planes a maximum gain close to 4.2 dB is observed at 0.8 and 1 GHz, lower than without a shield that induces weak losses. In the direction 180°, an attenuation higher than 20 dB for the main components in both planes is noticed.

2.3. Measurements

First experiments have been made on a dry and wet pure sand coming from the Seine valley in France. The dry sand has been deposited in a large box (height 740 mm, length 2 m, and width 1 m) inside our laboratory (see Figure 8(d)) and the wet sand (height 480 mm) has been found in the public square Perichaux (Paris 15) close to our laboratory after two weeks of bad weather. Both sands have not been compacted. The measurements have been made in the frequency domain $[0.05; 4]$ GHz (1601 samples) with a portable VNA ANRITSU MS 2026B. The intermediate frequency bandwidth (IFBW) has been defined to 500 Hz. A full two ports calibration has been made with 2 m length radio frequency cables. Each antenna has its own shield made of a box with an inner conductive coating and filled with a five-layered absorbing foam HPS 125 (distributed by EUROMC) with a total thickness of 150 mm.

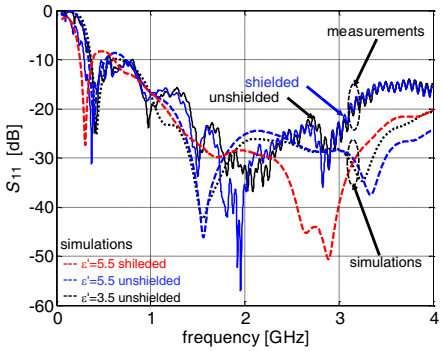

(a) measurements in a dry sand

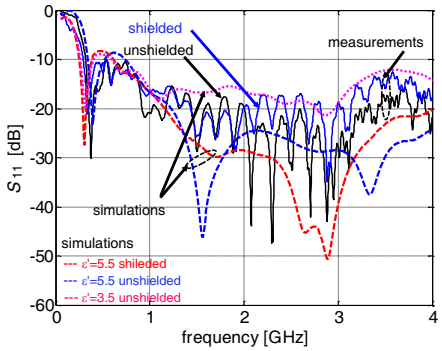

(b) measurements in a wet sand

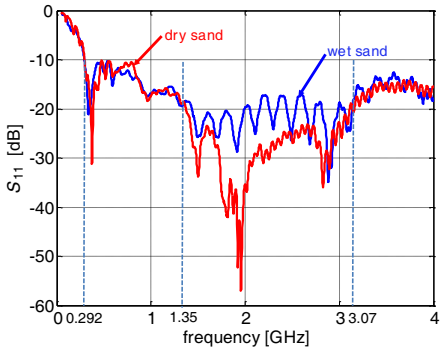

(c) measurements in a dry and wet sand (shielded case)

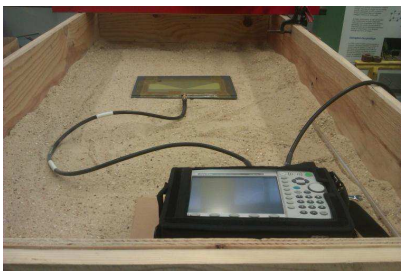

(d) laboratory box filled with dry sand

Figure 8. Comparison of theoretical and experimental return losses $S_{11\,\mathrm{dB}}(f)$; (a) In a dry and (b) a wet soil; (c) Comparison of measurement results only in a dry and a wet soil; (d) Experimental setup on a dry sand.

The comparison between experimental and theoretical reflection coefficients S_{11} in the presence of both types of sand is collected in Figures 8(a), 8(b), and 8(c). Considering the dry sand we remark in Figure 8(a) that the variations of the S_{11} experimental amplitudes with and without a shield appear similar; the presence of the shield slightly shifts S_{11} towards the left (lower frequency) because of the presence of a real permittivity in the absorbing material. In the unshielded case, among both values 3.5 and 5.5 for ε'_s, the theoretical S_{11} amplitude variations associated with $\varepsilon'_s = 3.5$ ($\sigma_s = 0.01\,\mathrm{S \cdot m^{-1}}$)

appear close to the experimental curve. Concerning the wet sand, we remark from Figure 8(b) that experimental S_{11} variations show more resonances than the theoretical results. The theoretical results associated with the shielded case with a soil value $\varepsilon'_s = 3.5$ ($\sigma_s = 0.01\,\mathrm{S\cdot m^{-1}}$) show amplitude variations close to the measurements. Moreover, we observe from Figure 8(c) that the wet sand introduces more dispersion in the return loss S_{11} as compared to the dry sand and particularly between frequencies 1.36 and 3.07 GHz. The lower frequency 291 MHz corresponding to $S_{11} = -10\,\mathrm{dB}$ does not appear modified when the sand is wet.

3. GPR SYSTEM

3.1. System Configurations

The radar system modeled, using FDTD simulations, is made of a pair of transmitting (external input impedance $50\,\Omega$) and receiving (impedance $10\,\mathrm{k}\Omega$ for voltage retrieval) shielded triangle bow-tie slot antennas positioned on the ground at an elevation $h = 1\,\mathrm{cm}$. Three main configurations have been considered: the parallel configuration (see Figure 9(a)) where the antennas are aligned along their larger dimension, the mirror configuration (see Figure 9(b)) where the antennas face each other symmetrically along their larger dimension, and the cross-polarization configuration (see Figure 9(c)) where the antennas are very close (a few cm) and are oriented at 90° to each other. For each of these configurations, the influence of the offset between both antennas (see Figures 10(a), 10(b) and 10(c)) on the amplitude of the transmission coefficient S_{21} (dB) considering a semi infinite homogeneous soil ($\varepsilon'_s = 5.5$; $\sigma_s = 0.01\,\mathrm{S\cdot m^{-1}}$) has been theoretically studied using FDTD simulations. The offset value results from a compromise between a weak direct path amplitude (low S_{21} in the first arrival times responsible for the clutter) and a sufficient high signal amplitude issued from the reflections inside the soil induced by the buried objects or dielectric contrasts.

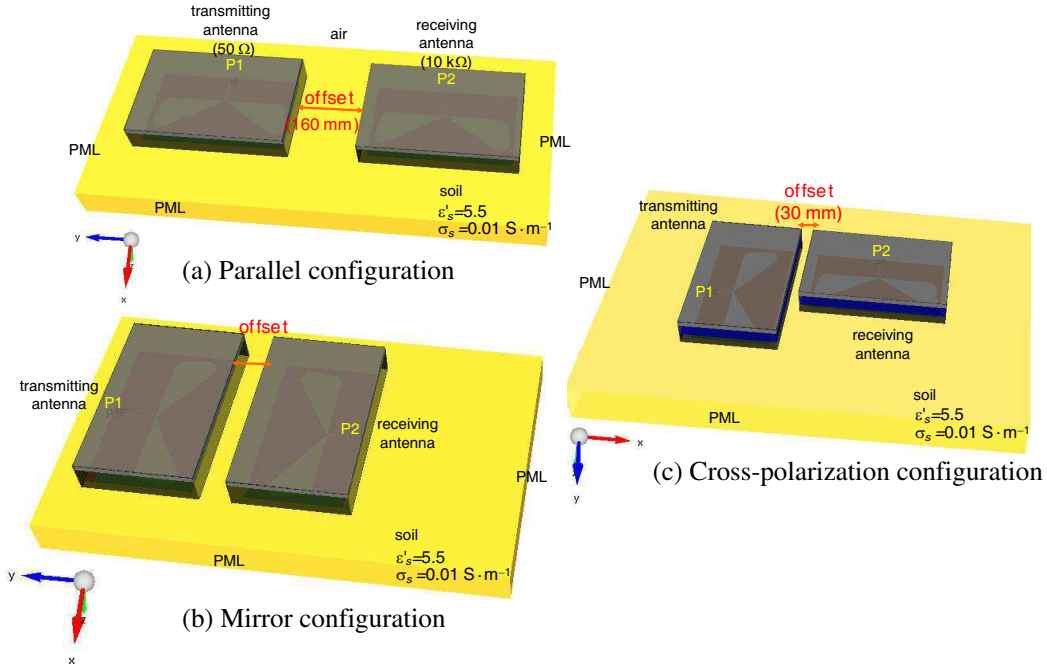

Figure 9. The three GPR configurations modeled using FDTD simulations: (a) The parallel configuration; (b) The mirror configuration, and (c) the cross-polarization configuration.

Comparing the transmission coefficient S_{21} (dB) in the parallel and mirror configurations (see Figures 10(a), and 10(b)) with offsets in the range $[0; 160]\,\mathrm{mm}$, we remark that the antenna coupling appears significantly lower in the parallel case, and particularly at frequencies lower than 1 GHz (15–20 dB lower). In the mirror configuration (see Figure 10(b)), a marked peak having the highest amplitude

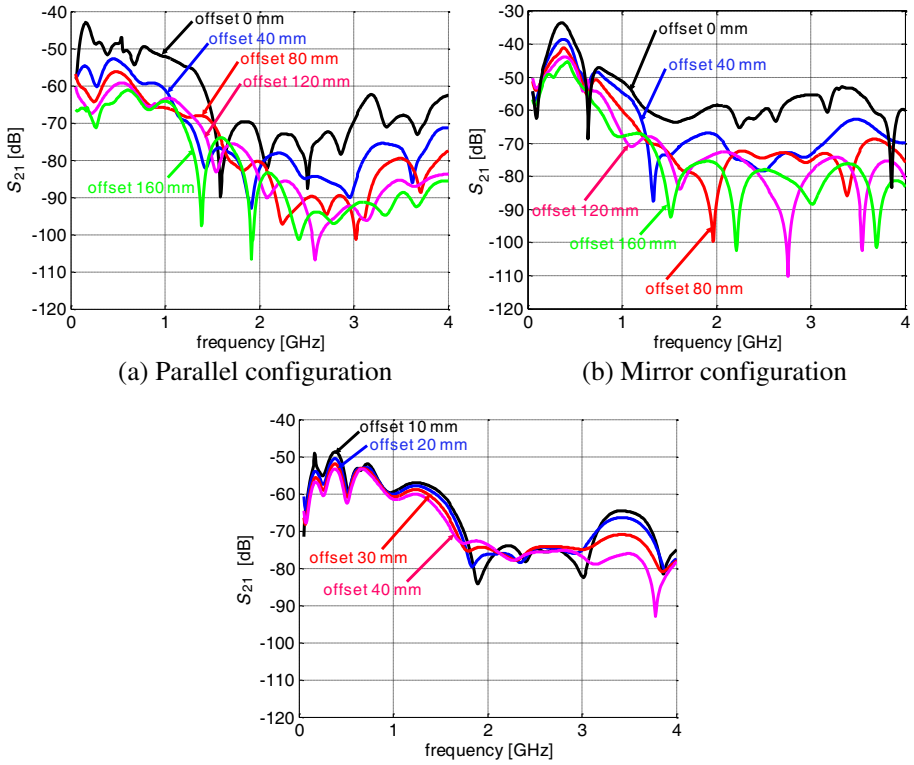

(a) Parallel configuration (b) Mirror configuration

(c) Cross-polarization configuration

Figure 10. Influence of the offset between antennas on the return loss $S_{11\,\mathrm{dB}}(f)$ issued from simulations; (a) In the parallel configuration, (b) in the mirror configuration, and (c) in the cross-polarization configuration.

is noticed between frequencies 0.350 and 0.430 GHz. As the ratio of the length to the width of the shielded antenna is 1.57, this could explain the lower coupling observed in the parallel case (antenna center-to-center distance more important). To reach an amplitude less than −40 dB, the offset must be greater than 40 mm. Thus, we have defined the offset 60 mm as the best compromise. Concerning the parallel configuration, an offset of 20 mm will be enough. In the cross-polarization configuration (see Figure 10(c)), the S_{21} (dB) amplitude appears lower than −50 dB for offsets greater than 10 mm, and consequently the isolation between both antennas is important.

3.2. Measurements in Several Configurations

Offset measurements have been made in the range $[0; 250]$ mm in the parallel and mirror configurations on the wet sand, such as visualized in Figures 11(a) and 11(b). The comparison of experimental and theoretical ($\varepsilon'_s = 5.5$; $\sigma_s = 0.01\,\mathrm{S{\cdot}m^{-1}}$) results highlights a higher coupling between both antennas in the measurements with a S_{21} (dB) amplitude difference around 12 dB for frequencies lower than 1.5 GHz. But, the dielectric properties of the wet sand are not known a priori. Thus, in both configurations, we have obtained the WARR (Wide Angle Reflection and Refraction) profiles where the transmitting antenna has been fixed and the receiving antenna is moving at a variable offset in the range $[50; 1000]$ mm with a step of 50 mm. From the complex transmission coefficients $\tilde{S}_{21}$ measured in the frequency band $[0.05; 4]$ GHz with a VNA, an apodisation of the data has been made to smoothly extend the band to 9 GHz. Then, a product of the spectrum of the excitation signal (first derivative of the Gaussian function, with duration 0.5 ns corresponding to 99% of the total energy, and $t_0 = 0.33$ ns) used in the FDTD simulations with the measured $\tilde{S}_{21}$ has been performed. Afterwards, the calculation of the inverse Fourier transform (IFFT) has led to time data.

Considering the simplified model with a planar layered medium, the travel time $t(y)$ along a raypath

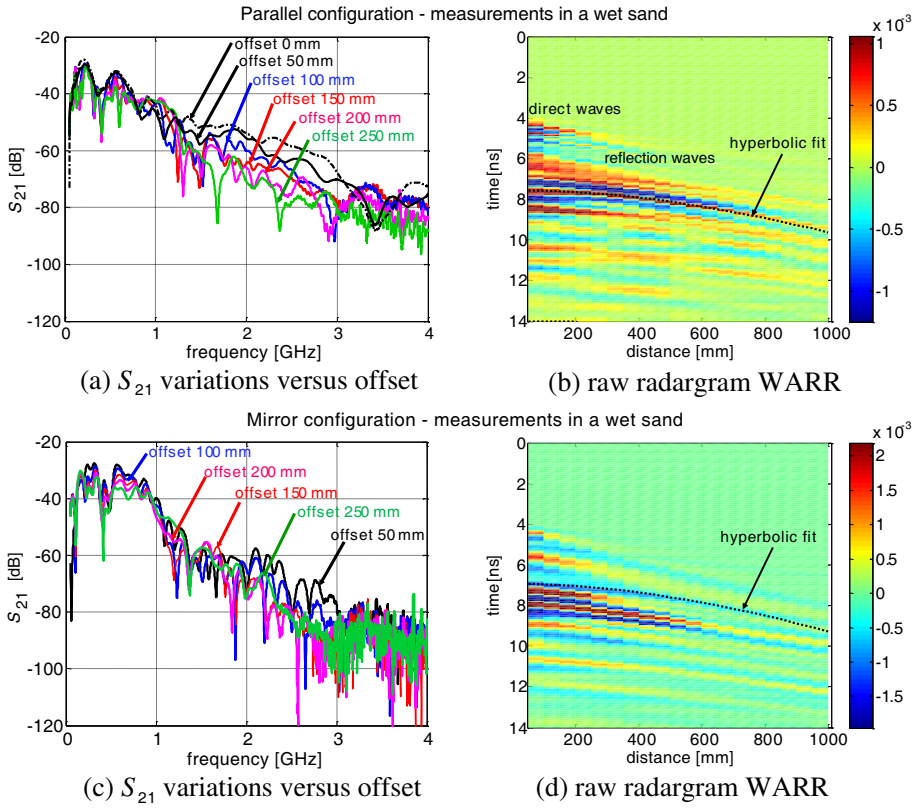

(a) S_{21} variations versus offset (b) raw radargram WARR

(c) S_{21} variations versus offset (d) raw radargram WARR

Figure 11. Influence the offset between antennas on the return loss $S_{11\,\mathrm{dB}}(f)$ issued measurements in a wet and non-compacted sand soil; in the parallel configuration (a) $S_{11\,\mathrm{dB}}(f)$ frequency variations, and (b) the associated radargram; in the mirror configuration (c) $S_{11\,\mathrm{dB}}(f)$ frequency variations, and (d) the associated radargram.

from the transmitter to the receiver after a bounce on a reflector and function of the offset is [10]:

$$t^2(y) = t^2(0) + y^2/v^2 \tag{1}$$

where $t(0)$ is twice the travel time along the vertical path, v is the velocity of the medium above the reflecting surface. The expression (1) has been used to firstly analyze each measured trace as a function of the offset in a range of velocities. An unnormalized cross correlation has been calculated according to [11] to estimate the velocity of the wet sand, and thus its real permittivity.

The experimental WARR cross-sections for both polarizations are thus presented in Figures 11(b) and 11(d); the time t_0 has not been calibrated that supposes to position adequately the antennas in air, in the far field zone and at a sufficient height from the ground. The coherence analysis has allowed to derive a first estimate of the relative real permittivity $\varepsilon'_{\mathrm{wet\,sand}} = 3.5$ for both polarizations. The associated hyperbolic curve (relation (1)) has been drawn in Figures 11(b) and 11(d).

3.3. Measurements of Local Discontinuities

The ability of the GPR system to detect small dielectric discontinuities in a soil has been preliminary validated in the wet sand and in the presence of two buried canonical objects (see Figure 12(a)): a water-filled pipe (diameter 25 mm) and vertical conductive strip (height 2 mm). The radargrams associated with both polarizations, parallel and mirror, are shown in Figures 12(b) and 12(c); the median value has been removed to reduce significantly the coupling between antennas. We remark that in the mirror configuration it appears quite difficult to detect the diffraction hyperbolas of both objects. However, in the parallel configuration, we remark that both hyperbolas are visible and even the one corresponding to the vertical strip. The vertical time difference between both hyperbolas, caused by a depth difference,

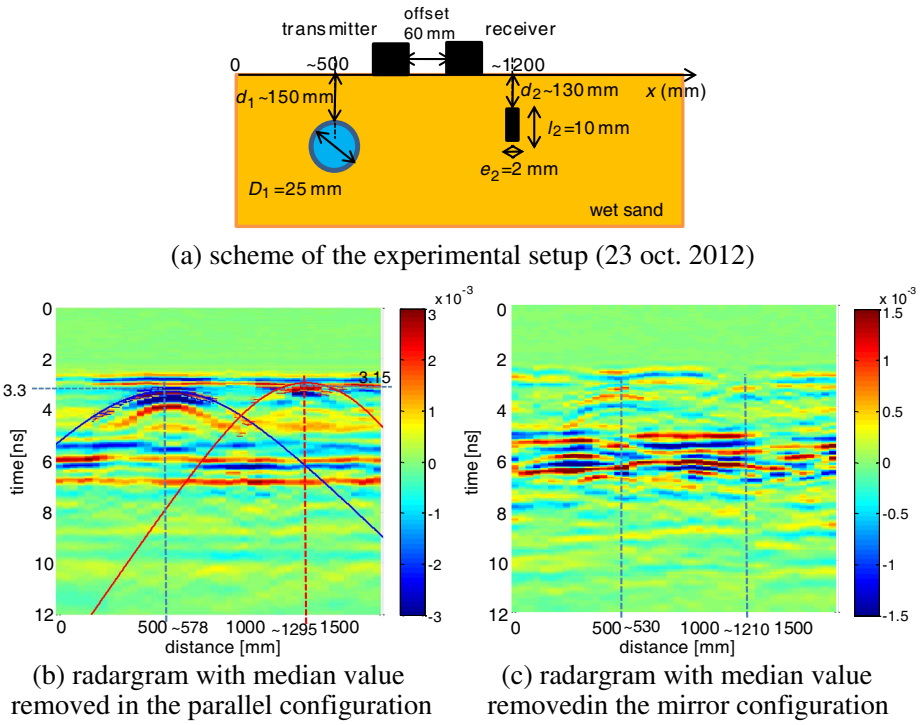

(a) scheme of the experimental setup (23 oct. 2012)

(b) radargram with median value removed in the parallel configuration

(c) radargram with median value removedin the mirror configuration

Figure 12. Measurements on the wet sand with two buried canonical objects: a water-filled pipe (diameter 25 mm) and vertical conductive strip (height 2 mm); (a) Geometry of the soil with the buried objects, and radargrams (b) in the parallel, and (c) in the mirror configurations.

is around 0.2 ns; this value agrees with the delay calculated using the hyperbola analytical relation involving a cylindrical object ($\varepsilon'_{\text{wet sand}} = 3.5$).

4. CONCLUSION

This work addresses the development and validation of a novel UWB triangle bowtie antenna for GPR applications, particularly in the civil engineering domain. The design of the antenna allows to improve its radiation characteristics and modify them if necessary. Fullwave FDTD simulations have allowed to study in details the antenna response in air and in the presence of a common soil ($\varepsilon'_s = 5.5$; $\sigma_s = 0.01\,\text{S}\cdot\text{m}^{-1}$) and to make comparison with experimental results. The polarization of the antennas has been particularly considered in a bistatic radar system in theory and in experimental situations to further examine the orientation of buried discontinuities or objects in the sub-surface. First measurements in the presence of canonical buried objects show the satisfying ability of the radar system to detect quite smaller than the antenna dimensions. Current studies aim at comparing measurements in the presence of different dielectric objects with full-wave simulations. Several data processing are currently developed that mainly concern clutter removing, automatic hyperbola detection, the slicing of the UWB into sub-bands to extract different types of information (penetration, shape, dielectric characteristics, frequency variations ...).

REFERENCES

1. Daniels, D. J., *Ground Penetrating Radar*, 2nd edition, The IEE, London, 2004.
2. Yelf, R. J., "Application of ground penetrating radar to civil and geotechnical engineering," *Electromagnetic Phenomena*, Vol. 7, No. 1, 102–117, 2007.
3. Diamanti, N. and D. Redman, "Field observations and numerical models of GPR response from vertical pavement cracks," *J. Applied Geophysics*, Vol. 81, 106–116, 2012.

4. Becker, J., D. Filipovic, H. Schantz, and S.-Y. Suh, "Ultra-wideband antennas," *International Journal of Antennas and Propagation*, Special Issue, Hindawi Publishing, 2008.
5. Wiesbeck, W., G. Adamiuk, and C. Sturm, "Basic properties and design principles of UWB antennas," *Proceedings of the IEEE*, Vol. 97, No. 2, 372–385, Feb. 2009.
6. Rahel, K., S. Bashir, and N. Fazal, "Review of techniques for designing printed antennas for UWB application," *International Journal of Sciences & Emerging Technologies*, Vol. 1, No. 2, 48–60, Feb. 2012.
7. Zheng, G., A. A. Kishk, A. W. Glisson, and A. B. Yakovlev, "Slot antenna fed by a CPW line with tapered transition," *Microwave and Opt. Technol. Letters*, Vol. 38, No. 6, 465–467, Sep. 2003.
8. Wu, C.-J., I.-F. Chen, and C.-M. Peng, "A dual polarization bow-tie slot antenna for broad band communications," *PIERS Proceedings*, 217–221, Marrakesh, Marocco, Mar. 20–23, 2011.
9. Atteia, G. E. and A. A. Shaalan, "Wideband partially-covered bowtie antenna for ground-penetrating radars," *Progress In Electromagnetics Research*, Vol. 71, 211–226, 2007.
10. Yilmaz, O., *Seismic Data Analysis: Processing, Inversion, and Interpretation of Seismic Data: Volume 1*, SEG Books, 2001.
11. Hamann, G. and J. Tronicke, "Assessing uncertainties in determining GPR ground wave velocities: An approach based on spectral velocity analysis," *6th International Workshop of Advanced Ground Penetrating Radar (IWAGPR)*, 1–5, Aachen, 2011.